Small Molecule Therapeutics

Molecular Cancer Therapeutics

The Irreversible Covalent Fibroblast Growth Factor Receptor Inhibitor PRN1371 Exhibits Sustained Inhibition of FGFR after Drug Clearance

Eleni Venetsanakos, Ken A. Brameld, Vernon T. Phan, Erik Verner, Timothy D. Owens, Yan Xing, Danny Tam, Jacob LaStant, Kwan Leung, Dane E. Karr, Ronald J. Hill, Mary E. Gerritsen, David M. Goldstein, Jens Oliver Funk, and J. Michael Bradshaw

Abstract

An increasing number of cancers are known to harbor mutations, translocations, or amplifications in the fibroblast growth factor receptor (FGFR) family of kinases. The FGFR inhibitors evaluated in clinical trials to date have shown promise at treating these cancers. Here, we describe PRN1371, an irreversible covalent inhibitor of FGFR1-4 targeting a cysteine within the kinase active site. PRN1371 demonstrated strong FGFR potency and excellent kinome-wide selectivity in a number of biochemical and cellular assays, including in various cancer cell lines exhibiting FGFR alterations. Furthermore, PRN1371 maintained FGFR inhibition *in vivo*, not only when circulating drug levels were high but also after the drug had been cleared from circulation, indicating the possibility of sustained FGFR inhibition in the clinic without the need for continuous drug exposure. Durable tumor regression was also obtained in multiple tumor xenografts and patient-derived tumor xenograft models and was sustained even using an intermittent dosing strategy that provided drug holidays. PRN1371 is currently under clinical investigation for treatment of patients with solid tumors. *Mol Cancer Ther; 16(12); 2668–76. ©2017 AACR.*

Introduction

The fibroblast growth factor receptors (FGFR) are a family of receptor tyrosine kinases (FGFR1, FGFR2, FGFR3, and FGFR4) important for many physiologic processes including development, angiogenesis, and homeostasis (1, 2). The binding of an FGF to an FGFR results in receptor dimerization and transphosphorylation of tyrosine kinase domains, leading to activation of downstream signaling pathways (3). Genetic alterations of FGFR, including mutations, fusions, and gene amplification, lead to aberrant signaling pathway activation and drive cancer growth. Genetic alterations of FGFR have been detected in multiple cancer types, including urothelial, squamous non–small cell lung (NSCLC), squamous head and neck cancer, cholangiocarcinoma, and breast cancer (4–6).

Emerging clinical data with multiple FGFR inhibitors have validated this target as a potential anticancer therapeutic. The first FGFR inhibitors to be assessed in the clinic were nonselective FGFR inhibitors, such as dovitinib and ponatinib, of which both on-target and off-target activities likely contributed to clinical responses. More recently, FGFR-selective inhibitors, such as BGJ398, have exhibited encouraging antitumor activity in clinical trials. Indeed, six confirmed partial responses were observed with BGJ398 at doses $\geq$ 100 mg in patients with FGFR1-amplified squamous NSCLC and FGFR3-mutant urothelial cancer patients in a phase I dose escalation trial (7).

Here, we describe the cellular and *in vivo* pharmacology of PRN1371, a selective irreversible covalent inhibitor of FGFR1-4. We demonstrate that PRN1371 exhibits strong potency and exquisite selectivity for FGFR1-4 in a variety of biochemical and cellular models. Furthermore, PRN1371 shows robust potency toward several FGFR point mutations. Sustained inhibition of phospho-FGFR is observed in response to PRN1371 dosing, despite fast clearance of the compound from the plasma. PRN1371 also demonstrates strong antitumor growth activity in FGFR-driven xenograft models, including patient-derived xenografts, in response to both continuous and intermittent dosing.

Materials and Methods

Cell lines and reagents

The gastric cancer cell line SNU16, the bladder cell lines RT4 and RT112, and the HCT116 colon cancer line were purchased from ATCC. AN3CA, LI7, SNU878, JHH7, Hep3B, NCI-H716, and OPM2 cell lines were characterized by Crown Bioscience. SNU16, RT112, NCI-H716, LI7, SNU878, and OPM2 were cultured in RPMI-1640 medium with 10% fetal bovine serum (FBS, Gibco Cat#26140-079). RT4 and HCT116 were cultured in McCoy's 5a Medium Modified with 10% FBS. AN3CA was cultured in MEM with 10% FBS, 1 mmol/L sodium pyruvate, and 0.1 mmol/L NEAA. JHH7 was cultured in William's E with 10% FBS plus

Principia Biopharma, South San Francisco, California.

Note: Supplementary data for this article are available at Molecular Cancer Therapeutics Online (http://mct.aacrjournals.org/).

Corresponding Author: J. Michael Bradshaw, Principia Biopharma, 400 East Jamie Court, Suite 302, South San Francisco, CA 94080. Phone: 650-416-7713; Fax: 650-266-3436; E-mail: michael.bradshaw@principiabio.com

doi: 10.1158/1535-7163.MCT-17-0309

0.01 mmol/L NEAA. Hep3B were cultured in EMEM with 10% FBS and 0.1 mmol/L NEAA. HUVECs (Genlantis Cat#PH20005N) were maintained in endothelial cell growth medium (Genlantis Cat#PM211500) containing 10% FBS. Cells were maintained in standard culture conditions of 37°C, 5% CO_2 and 95% humidity and were kept in culture for up to 15 to 20 passages. Cell lines were obtained between the years 2013 and 2015. PRN1371 and the fluorescent probe were synthesized as described (8).

Kinase assays

Enzyme inhibition was determined using a Caliper capillary electrophoresis system that separates phosphorylated and non-phosphorylated peptides on the basis of charge. Different concentrations of inhibitor were first preincubated with enzyme for 15 minutes. The reaction was initiated with addition of peptide substrate, ATP, and Mg^{2+} and incubated at 25°C for 3 hours. To stop the reaction, the mixture was quenched with EDTA. The buffer was 100 mmol/L HEPES, pH 7.5, 0.1% BSA, 0.01% Triton X-100, 1 mmol/L DTT, 10 mmol/L $MgCl_2$, 10 mmol/L sodium orthovanadate, 10 μmol/L beta-glycerophosphate, and 1% DMSO. The ATP concentration of the reaction was at the predetermined value of the K_m for ATP. IC_{50}s represent the mean values ± SD ($n = 5$). For dialysis studies, 50 nmol/L inhibitor is incubated with 2 nmol/L enzyme for 1 hour at 22°C. Control samples with no added inhibitor were included for normalization. Dialysis occurred for either 24 hours (FGFR3, FGFR4, and CSF1R) or 72 hours (FGFR1 and FGFR2) with a change of dialysis buffer twice daily. Following dialysis, enzyme activity was assessed as described above and reported as the percentage enzyme activity compared to a noncompound treated control ($n = 4$ for FGFR1 and FGFR4, otherwise $n = 2$). All enzyme inhibition data were acquired by Nanosyn, Inc. (www.nanosyn.com). Kinase selectivity was also evaluated using the Nanosyn 250 kinase panel.

Ba/F3 cell line proliferation

In the Ba/F3 studies, a recombinant kinase was transduced into an engineered Ba/F3 cell line which became dependent upon the kinase activity for IL3-independent survival. Cells were first plated at 5,000 cells per well in a 384-well plate. An inhibitor concentration series was then added, and cells were cultured for 48 hours at 37°C. Cell viability was typically measured using CellTiter-Glo (Promega), which measures intracellular ATP concentration as a surrogate marker for viability. IC_{50} values represent the mean ± SD ($n = 4$ for FGFR4 and CSF1R, otherwise $n = 2$). Ba/F3 cell proliferation studies were performed by Advanced Cellular Dynamics (http://acdynamics.com/).

ERK phosphorylation in HUVECs

Human umbilical vein endothelial cells (HUVEC) were incubated in media supplemented with 10% FBS and seeded at 30,000 cells per well in a 96-well plate overnight. HUVECs were then transferred into serum-free media 1 hour before compound treatment. A compound concentration series was added to cells and incubated for 1 hour at 37°C. Cells were then stimulated with either 50 ng/mL of FGF2 (R&D Systems Cat#233-FG-025) or 50 ng/mL of VEGF (R&D Systems Cat#293-VE-050) for 10 minutes. Ice-cold PBS was added to stop the reaction, and cells were washed three times to remove media. A pERK SureFire kit (PerkinElmer) that utilizes Alphascreen technology was used to determine ERK phosphorylation using an Envision multilabel plate reader (PerkinElmer). IC_{50} values represent the mean ± SD ($n = 12$ for FGF stimulation and $n = 2$ for VEGF stimulation).

FGFR target occupancy in SNU16 cells

SNU16 gastric cancer cells were utilized to directly measure occupancy of PRN1371 toward FGFR using a BODIPY-labeled occupancy probe. A total of 500,000 cells per well were added to each well of a 24-well plate. After a 1-hour compound incubation, cells were treated with a final concentration of 1 μmol/L of BODIPY-labeled occupancy probe for 1 hours. Cells were collected, washed, and lysed with CelLytic M lysis buffer (Sigma) on ice for 15 minutes. Samples were evaluated using SDS-PAGE and evaluated using in-gel fluorescence with a Typhoon gel image scanner. Total FGFR2 was also evaluated using immunoblotting with a mouse anti-FGFR2 antibody (1:500 dilution) from R&D Systems (Cat#MAB6841). The IC_{50} value represents the mean ± SD ($n = 2$) of independent experiments. In order to assess the durability of inhibitors to FGFR2 following inhibitor washout, 1 million cells per well were plated in a 12-well plate. Cycloheximide was then added to each well at a concentration of 5 μg/mL and utilized in the media throughout subsequent steps. Test compound was added to cells at a final concentration of 40 nmol/L and incubated for 1 hour to facilitate FGFR2 binding. Cells were subsequently washed 3 times and incubated for 1 or 4 hours. Cell lysates were generated and subsequently evaluated for both total FGFR2 and phospho-FGFR2 by Western blotting.

FGFR phosphorylation assessment

To assess the potency of PRN1371 toward inhibiting FGFR phosphorylation, SNU16 cells were first incubated with various concentrations of PRN1371 for 1 hour. Cells were then stimulated with 50 ng/mL bFGF for 10 minutes. SNU16 cell lysates were evaluated by SDS-PAGE and immunoblotting using a rabbit anti-pFGFR2 antibody (Cellular Signaling Technology Cat#3471S) and a mouse anti-FGFR2 antibody (R&D Systems Cat#MAB6841). The IC_{50} value represents the mean ± SD ($n = 2$) of independent experiments.

Cell proliferation

Cells were first seeded into 384-well plates and compounds were added such that the highest final compound concentration is 5 μmol/L. Cells were incubated with compound for 72 hours at 37°C. To detect viability, the Presto-Blue cell viability reagent (Life Technologies Cat#A13261) was added per manufacturer's instructions. Plates were read using an Analyst HT with a fluorescent mode used 530 nm excitation and 590 nm emission. The IC_{50} values represent the mean ± SD ($n = 3$ for SNU16 cells, otherwise $n = 2$) of independent experiments. For the SNU16 gastric cancer cell line, inhibition of proliferation was also assessed using BrdUrd incorporation with a BrdUrd ELISA kit (Abcam Cat#ab126572). Here, the IC_{50} value represents the mean ± SD ($n = 4$).

Apoptosis induction assays

Cells were cultured in 384-well plates for 24 hours at 37°C and incubated with an inhibitor dilution series for 42 hours. Cells were evaluated for viability, necrosis, and apoptosis simultaneously using the triplex ApoTox-Glo assay kit (Promega). Apoptosis was measured using a substrate of caspase 3 and 7, which are activated during apoptosis. The caspase 3 and 7 detection

reagent was added for 30 minutes, and plates were then read using an Analyst HT plate reader in luminescence mode.

Xenograft mouse studies

For xenograft studies with SNU16 or RT4 cells, a suspension of 1×10^7 cells were injected at the upper right back of 7-week-old female nude mice (Crown Bioscience). For PDX xenograft studies, tumor fragments from stock mice inoculated with selected primary human cancer tissues were harvested and used to inoculate mice. Each mouse was inoculated subcutaneously into the right flank with a 2 to 4 mm diameter tumor fragment. The average age of female mice used in PDX studies was 10 to 12 weeks (Crown Bioscience). The care and treatment of experimental animals were in accordance with institutional guidelines. Mice were randomized ($n = 10$ per group) once the mean tumor volume had reached an average tumor size of ~150–180 mm^3 and there were no exclusion criteria. PRN1371 was suspended in 0.5% methylcellulose w/w in deionized water. Tumor volumes were measured three times weekly using a caliper and the volume was expressed in mm^3 using the formula $V = 0.5\ a \times b^2$, where a and b are the long and short diameters of the tumor, respectively. Tumor weight was measured at study termination.

Statistical analysis

Data analysis was performed using GraphPad Prism software. Unless noted otherwise, error bars in figures represent the standard error of independent determinations.

Results

Potent, selective, and covalent inhibition of FGFR1, FGFR2, FGFR3, and FGFR4 by PRN1371

We targeted a rare cysteine (Cys 486 of FGFR1) in the ATP binding site of FGFR1, FGFR2, FGFR3, and FGFR4 in order to identify a covalent and selective inhibitor of the FGFR family of kinases. Guided by structure-based design, several chemical scaffolds coupled to cysteine-reactive warheads were synthesized and characterized. Optimization of an attractive lead series was guided by both an FGFR1 enzyme activity assay and an FGFR1 biochemical occupancy assay that provided a readout on covalent cysteine engagement; the detailed SAR and medicinal chemistry involved in this work has been published elsewhere (8). The effort culminated in the identification of PRN1371 (Fig. 1A) as a potent, selective, and covalent inhibitor of FGFR1, FGFR2, FGFR3, and FGFR4.

The potency of PRN1371 was assessed in biochemical enzyme inhibition assays. PRN1371 demonstrated strong potency toward FGFR1 ($IC_{50} = 0.7 \pm 0.1$ nmol/L), FGFR2 ($IC_{50} = 1.3 \pm 0.2$ nmol/L), and FGFR3 ($IC_{50} = 4.1 \pm 0.7$ nmol/L), with slightly weaker potency toward FGFR4 ($IC_{50} = 19.3 \pm 4.7$ nmol/L) (Fig. 1B). Strong selectivity for the FGFR family over VEGFR2 was observed (VEGFR2 $IC_{50} = 705 \pm 63$ nmol/L) (Fig. 1B). To evaluate kinome-wide selectivity, PRN1371 was tested at 1 μmol/L and 0.1 μmol/L in a 250 kinase enzyme inhibition panel. Excellent selectivity was observed with only a single kinase outside the FGFR family,

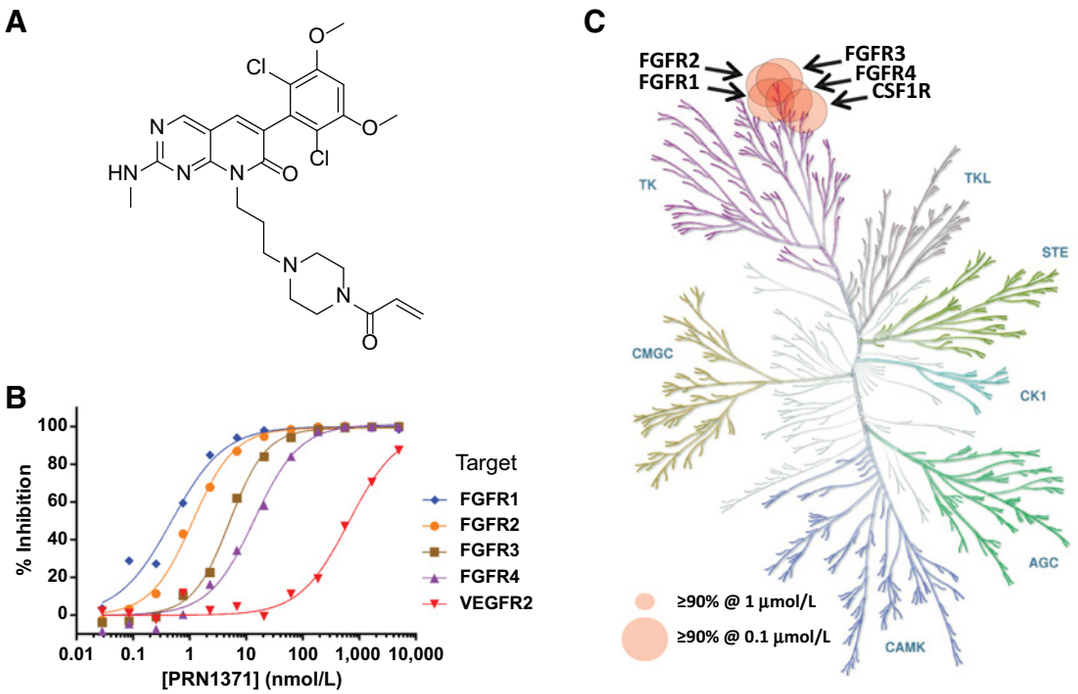

Figure 1.

Biochemical potency and selectivity of PRN1371. **A,** Chemical structure of PRN1371. **B,** Enzymatic inhibition of PRN1371 toward FGFR1, FGFR2, FGFR3, FGFR4, and VEGFR2. Shown is the percentage of inhibition of enzymatic activity versus [PRN1371] for a representative experiment ($n = 5$). **C,** Kinase selectivity of PRN1371. Circles indicate kinases that demonstrate inhibition ≥90% inhibition at 1 μmol/L, with larger-sized circles indicating kinases that also showed ≥90% inhibition at 0.1 μmol/L. Each of the 5 kinases inhibited by PRN1371 (FGFR1, FGFR2, FGFR3, FGFR4, CSF1R) is indicated. Data reproduced with permission from Brameld et al. (8). Copyright 2017 American Chemical Society. Kinome representation was reproduced courtesy of Cell Signaling Technology (www.cellsignal.com).

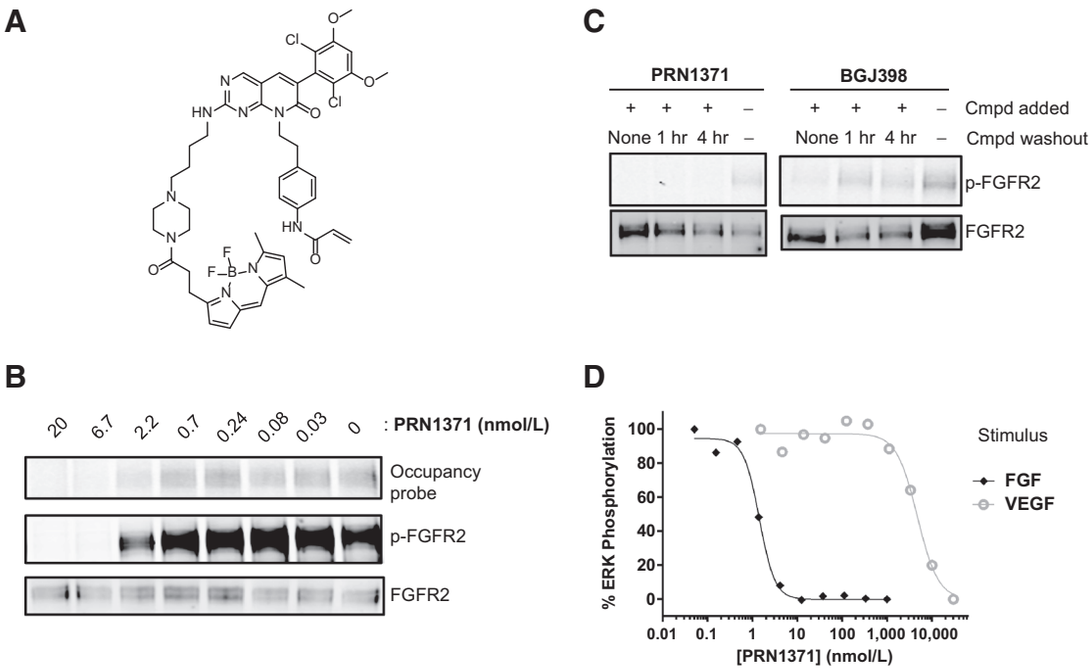

Figure 2.

Potent and durable engagement of FGFR in cells by PRN1371. **A,** Compound structure of the BODIPY-labeled FGFR occupancy probe. **B,** PRN1371 inhibition of FGFR2 in SNU16 cells. Top, In-gel fluorescence derived from occupancy probe binding to FGFR2 and the concentration-dependent inhibition of this signal by preincubation of cells with PRN1371. Middle and bottom, Western blots of either pFGFR2 (middle) or total FGFR2 (bottom) evaluated after incubation of SNU16 cells with the indicated concentration of PRN1371. **C,** PRN1371 sustained inhibition of FGFR2 phosphorylation following inhibitor washout. Shown are Western blots of pFGFR2 (top) or total FGFR2 (bottom) evaluated after washout of either PRN1371 (left) or BGJ398 (right) from cells. **D,** PRN1371 potently blocked FGF-stimulated but not VEGF-stimulated ERK phosphorylation in HUVEC cells. HUVECs were treated with different concentrations of PRN1371 and then stimulated with either 50 ng/mL bFGF or 50 ng/mL VEGF. ERK phosphorylation was evaluated using the AlphaLISA pERK SureFire Kit. Shown is the percentage of ERK phosphorylation versus [PRN1371] for a representative experiment ($n = 12$ for FGF stimulation and $n = 2$ for VEGF stimulation).

CSF1R, demonstrating greater than 90% inhibition at 1 μmol/L of PRN1371 (Fig. 1C). We further characterized the potency of all kinases that demonstrated >50% inhibition at 1 μmol/L PRN1371 in the 250 kinase panel. No additional kinases beyond FGFR1, FGFR2, FGFR3, FGFR4, and CSF1R demonstrated an IC_{50} < 200 nmol/L toward PRN1371 (8).

To establish that PRN1371 binding is covalent, dialysis studies were performed. FGFR isoforms were incubated with PRN1371 followed by dialysis that removes unbound and reversibly bound inhibitor. We found that PRN1371 demonstrated sustained inhibition of FGFR1, FGFR2, FGFR3, and FGFR4 following dialysis, indicating irreversible covalent binding of PRN1371 to all 4 FGFR isoforms (Supplementary Table S1). In contrast, the control FGFR inhibitor BGJ398 failed to sustain inhibition of FGFR, which is consistent with its reversible noncovalent binding mechanism (Supplementary Table S1). We have also previously shown that PRN1371 demonstrates time-dependent enzyme inhibition of FGFR1-4 and sustains inhibition of fluorescent probe binding to the FGFR active site, further validating covalent FGFR engagement (8). CSF1R, the only kinase outside the FGFR family inhibited by PRN1371, was also studied using dialysis. CSF1R does not contain a cysteine at the same location within the ATP binding site as the FGFR family so was not anticipated to demonstrate sustained inhibition by PRN1371. As expected, activity of CSF1R fully recovered following removal of PRN1371 by dialysis (Supplementary Table S1).

PRN1371 exhibits potent and durable pathway inhibition

The effect of PRN1371 on the FGFR signaling pathway was next studied in cells. Cellular activity was first assessed in the SNU16 gastric cancer cell line, which exhibits an amplification of FGFR2. A novel, BODIPY-labeled FGFR occupancy probe (Fig. 2A) was identified that covalently labeled FGFR2 in the SNU16 cells and could be assessed using in-gel fluorescence. It was then explored what concentration of PRN1371 was required to block probe binding. Preincubation of SNU16 cells with a concentration series of PRN1371 prior to addition of the occupancy probe blocked binding of the probe with an IC_{50} of 2.1 ± 1.4 nmol/L (Fig. 2B). Because autophosphorylation of FGFR is dependent on FGFR kinase activity, it was hypothesized that PRN1371 would inhibit FGFR autophosphorylation. Indeed, PRN1371 blocked bFGF-stimulated autophosphorylation of FGFR2 in SNU16 cells with an IC_{50} of 2.9 ± 1.4 nmol/L, as assessed by Western blotting (Fig. 2B).

To confirm the covalent mechanism of action of PRN1371 within cells, a cellular washout study was performed. PRN1371 at a concentration of 40 nmol/L was incubated with cycloheximide-treated, FGFR2-amplified SNU16 gastric cancer cells. The noncovalent inhibitor BGJ398 was also included at 40 nmol/L as a control. The cells were extensively washed to remove any inhibitor not bound to FGFR2, then 1 or 4 hours was allowed to elapse to allow for the possibility of compound dissociation from the target, and finally FGFR2 phosphorylation was evaluated using

Table 1. Potency of PRN1371 in Ba/F3 cells

Target	IC_{50} ± SD (nmol/L)
FGFR1	0.7 ± 0.02
FGFR1 (V561M)	34.5 ± 2.0
FGFR2	0.7, <0.6[a]
FGFR2 (N550K)	3.9 ± 1.2
FGFR2 (K660E)	1.3, <0.6[a]
FGFR2 (K660N)	0.8, <0.6[a]
FGFR3	2.5 ± 0.5
FGFR3 (K650M)	3.4 ± 0.5
FGFR4	49.8 ± 26.0
VEGFR2	>2000
CSF1R	1,224 ± 792

[a]Data from two independent determinations.

Western blotting. PRN1371, but not BGJ398, sustained the ability to block FGFR2 autophosphorylation following inhibitor washout (Fig. 2C), indicating covalent binding of PRN1371 to FGFR2 in cells.

In order to evaluate the effect of PRN1371 on downstream pathway activation, human umbilical vein endothelial cells (HUVECs) primarily expressing FGFR1 were stimulated with basic FGF (bFGF) followed by evaluation of ERK phosphorylation using Alphascreen technology. PRN1371 inhibited bFGF-stimulated ERK phosphorylation with an IC_{50} of 1.5 ± 0.7 nmol/L (Fig. 2D). In contrast, ERK phosphorylation in HUVECs stimulated with VEGF was only weakly inhibited by PRN1371 with an IC_{50} of 6,350 ± 2,009 nmol/L, corroborating the strong selectivity of PRN1371 for FGFR over VEGFR2 observed biochemically.

PRN1371 exhibits robust antiproliferative activity

The antiproliferative activity of PRN1371 toward the FGFR isoforms was assessed using the Ba/F3 system. Briefly, Ba/F3 cells were modified to express a recombinant kinase and were thus rendered dependent on the activity of this recombinant kinase for proliferation. PRN1371 inhibited the proliferation of Ba/F3 cells expressing FGFR1, FGFR2, FGFR3, and FGFR4 with IC_{50} values of 0.7 ± 0.02 nmol/L, 0.7 ± 0.1 nmol/L, 2.5 ± 0.5 nmol/L, and 49.8 ± 26.0 nmol/L, respectively (Table 1). In contrast, PRN1371 was inactive toward VEGFR2 in the Ba/F3 system (Table 1). Furthermore, PRN1371 only weakly inhibited proliferation of CSF1R-expressing Ba/F3 cells with an IC_{50} of 1,224 ± 792 nmol/L.

Multiple FGFR mutations have been identified in the extracellular, transmembrane, and kinase domains, which can lead to tyrosine kinase activation (4). To establish the potency of PRN1371 against FGFR mutations, we utilized the Ba/F3 system to characterize available FGFR2 and FGFR3 mutations, including FGFR2-K660E, FGFR2-K660N, FGFR2-N550K, and FGFR3-K650M. We found that PRN1371 potently inhibited each of these mutations with low, single-digit nanomolar IC_{50} values (Table 1).

The antiproliferative activity of PRN1371 was assessed in various cancer cell lines exhibiting FGFR pathway alterations and also a cancer cell line that is wild-type for FGFR (Table 2). The cell lines tested included bladder, liver, endometrial, colorectal, and gastric cancer cell lines harboring mutations, fusions, or amplification of FGFR, including cancer cell lines exhibiting FGF19 amplification. PRN1371 strongly inhibited proliferation of the cancer cell lines with low IC_{50} values, including RT4 (IC_{50} = 4.0 ± 1.7 nmol/L), RT112 (IC_{50} = 4.1 ± 1.4 nmol/L), NCI-H716 (IC_{50} = 2.0 ± 1.7 nmol/L), and SNU16 (IC_{50} = 2.6 ± 2.2 nmol/L) cells. From examination of the RT4 cell line data, it was noted that potency did not necessarily correlate with the maximum level of inhibition (Table 2). Furthermore, the HCT116 colon carcinoma line, which is wild-type for FGFR, was not inhibited by PRN1371 (Table 2). Inhibition of SNU16 cell proliferation by PRN1371 was studied as described above using a cell viability reagent and also using BrdUrd incorporation (Supplementary Fig. S1) and a comparable inhibition of proliferation was observed using both approaches.

To further characterize the cellular effects of PRN1371, we tested the hypothesis that PRN1371 can induce apoptosis in cells that contain FGFR pathway alterations. The activation of caspase 3 and 7 upon treatment with different concentrations of PRN1371 was monitored in both SNU16 and RT4 cancer cell lines as an indicator of apoptosis. A dose-dependent activation of caspase 3 and 7 was observed in both cell lines, with EC_{50} of 15.9 ± 3.0 nmol/L and 11.8 ± 4.0 nmol/L for activation in RT4 and SNU16 cells, respectively (Supplementary Fig. S2).

PRN1371 demonstrates prolonged FGFR inhibition *in vivo*

An advantage of a covalent mechanism of action is to enable sustained duration of signaling pathway inhibition. In order to assess this *in vivo*, PRN1371 was orally administered to SNU16 tumor–bearing BALB/c mice. Mice were orally dosed with either 2.5 mg/kg or 10 mg/kg daily for 4 days, and tumors were harvested for analysis of phospho-FGFR2 at various time points following the fourth dose. Plasma was also collected for analysis of circulating drug levels. Strong inhibition of phospho-FGFR2 was observed up to 4 hours post last dose at 2.5 mg/kg and up to 8

Table 2. Antiproliferative activity of PRN1371 across cancer cell lines

Cell line	Tumor type	FGFR pathway alteration	PRN1371 IC_{50} (nmol/L) ± SD	Maximum inhibition (%)
RT4	Bladder, transitional cell carcinoma	FGFR3:TACC3 fusion	4.0 ± 1.7	56.1
RT112	Bladder, transitional cell carcinoma	FGFR3:TACC3 fusion	4.1 ± 1.4	84.4
ANC3A	Endometrial adenocarcinoma	FGFR2-N549K mutation	43.3 ± 4.0	83.6
L17	Hepatocellular carcinoma	FGF19 amplification	33.1 ± 9.1	91.7
SNU878	Hepatocellular carcinoma	FGF19 amplification	120 ± 6	98.5
JHH7	Hepatocellular carcinoma	FGF19 amplification	231 ± 40	80.5
Hep3B	Hepatocellular carcinoma	FGF19 amplification	6.0 ± 4.9	93.8
NCI-H716	Colorectal adenocarcinoma	FGFR2 amplification/C3 truncation and FGFR2:COL14A1 fusion	2.0 ± 1.7	98.0
SNU16	Gastric carcinoma	FGFR2 amplification/C3 truncation	2.6 ± 2.2	88.5
OPM2	Multiple myeloma	FGFR3 translocation (t4;14) and FGFR3-K562E mutation	14.0 ± 0.1	95.5
HCT116	Colon carcinoma	Wild-type	4,819 ± 1,858	77.8

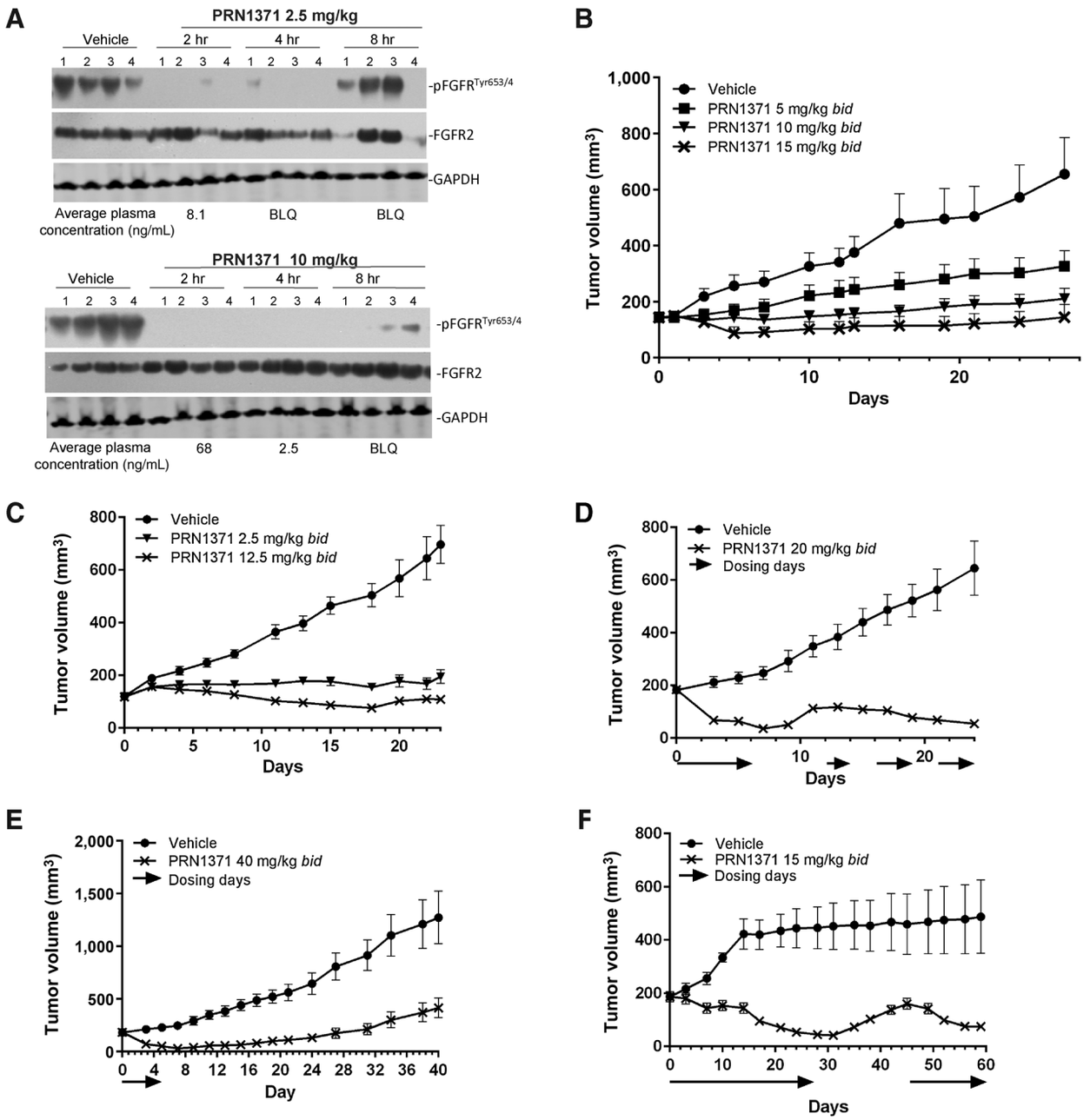

Figure 3.

PRN1371 exhibits sustained pFGFR inhibition *in vivo* and demonstrates potent efficacy in xenograft and PDX models. **A,** SNU16 tumor–bearing mice were orally dosed daily for 4 days and xenograft tumors assessed for phospho-FGFR at 2, 4, and 8 hours after final dose. Western blot analysis for phospho-FGFR, total-FGFR, and GADPH was assessed. Average plasma concentrations in ng/mL for each time point were also reported. **B,** SNU16 tumor–bearing mice were orally administered with vehicle or the indicated concentration of PRN1371 twice daily (circles: vehicle; crosses, squares or triangles: PRN1371; mean ± SEM, $n = 10$). **C,** RT4 tumor–bearing mice were orally administered with vehicle or the indicated concentration of PRN1371 twice daily (mean ± SEM, $n = 10$). **D,** SNU16 tumor–bearing mice were administered with either vehicle or with PRN1371 twice daily at 20 mg/kg with an intermittent dosing regimen with the days of dosing indicated by arrows (mean ± SD, $n = 10$). **E,** SNU16 tumor–bearing mice were administered with either vehicle or with PRN1371 twice daily at 40 mg/kg for the first 5 days of the study only (mean ± SEM, $n = 10$). **F,** Mice bearing the PDX model LI1055 were administered with either vehicle or PRN1371 twice daily at 15 mg/kg for 27 days. Dosing was discontinued on day 28 for 16 days, before reinitiating dosing at 10 mg/kg twice daily for another 14 days (mean ± SEM, $n = 10$). In all *in vivo* studies, tumor volume and body weight change were then measured three times per week for duration of study.

Table 3. *In vivo* efficacy of PRN1371 in patient-derived xenograft models

PDX name	Tumor type	FGFR alteration	Tumor growth inhibition
LU0299	Squamous NSCLC	FGFR1 Amp + High Expr	96.1%
LU1215	Lung adenocarcinoma	FGFR1 Amp + High Expr	64.6%
LU2504	Squamous NSCLC	FGFR1 Amp + High Expr	59.5%
LU1429	Squamous NSCLC	FGFR3 Amp + High Expr	28.2%
LU6429	Squamous NSCLC	FGFR2 Amp	67.5%
BN2289	Anaplastic oligodendroglioma	FGFR3:TACC3 fusion	100.3% (Regression −3%)
LI0155	Liver (mixed liver, HCC, and adenocarcinoma of bile duct)	FGFR2:CCDC6 fusion FGFR4 mutation	>100% (Regression −76%)
BR1115	Breast	FGFR2 Amp + High Expr; FGFR2:GAB2 fusion	60.6%

hours post last dose in half the animals at 10 mg/kg (Fig. 3A). The average plasma concentration of PRN1371 was 8.1 and 68 ng/mL at 2 hours post final dose at 2.5 and 10 mg/kg, respectively, and was rapidly cleared by 4 hours in both dose groups (Fig. 3A). In summary, inhibition of phospho-FGFR was sustained in the SNU16 tumors beyond clearance of compound from circulation in tumor-bearing mice.

Antitumor activity of PRN1371 in mouse xenograft models

The efficacy of PRN1371 was assessed in various tumor xenograft models. The first xenograft model to be assessed was SNU16, a human gastric cancer cell line that harbors an amplification of FGFR2. SNU16 tumor–bearing mice were orally dosed with PRN1371 at 5, 10, and 15 mg/kg twice a day (b.i.d.) and exhibited dose-dependent tumor growth inhibition (TGI) at 50%, 68%, and 78%, respectively (Fig. 3B). The efficacy of PRN1371 was also explored in a second xenograft model, RT4, a human bladder cancer cell line exhibiting the FGFR3:TACC3 fusion. PRN1371 was orally dosed at 2.5 mg/kg and 12.5 mg/kg b.i.d. in RT4 tumor–bearing mice. Potent tumor growth inhibition of 72% was observed at 2.5 mg/kg and regression of −8% was observed at the higher dose of 12.5 mg/kg (Fig. 3C). The dosing regimens were well tolerated, with no significant body weight loss. In summary, PRN1371 demonstrated dose-dependent antitumor activity in both xenograft models.

To further understand the efficacy of PRN1371, we investigated the antitumor activity of PRN1371 in a mouse xenograft model using an intermittent dosing regimen. The SNU16 tumor xenograft model was orally dosed with two different regimens; in the first regimen assessed, SNU16 tumor–bearing mice were orally dosed with 20 mg/kg b.i.d. for 6 days on, 5 days off followed by a recurring cycle of 3.5 days on/2 days off. On day 28, the final day of the study, tumor regression of −70% was measured (Fig. 3D). In the second dosing regimen, SNU16 tumor–bearing mice were treated with a high bolus oral dose of 40 mg/kg b.i.d. for only 5 days, following by monitoring of tumor size for the study period. In the high bolus study, tumor regression of −28% was observed on day 7 of the study period with a TGI of 79% on day 40 (Fig. 3E). It should be noted that significant body weight loss was observed on day 5 with the high bolus dose; however, all mice recovered body weight during the drug holiday, which was maintained up to day 40. These observations suggest that either an intermittent dosing regimen with a moderate dose or a short dosing period of a high dose of PRN1371 can result in significant antitumor activity *in vivo*.

Patient-derived xenograft (PDX) models have been demonstrated to exhibit a high predictive value for targeted therapeutics in oncology (9, 10). Thus, we selected a range of PDX tumors to assess with PRN1371, based on the following criteria: for lung PDX models, high ($\geq$4) copy number of FGFR1 or FGFR3 and high expression of FGFR1 or FGFR3 (> mean of analyzed tumors) or high copy number of FGFR2; for other PDX tumor types, presence of an FGFR fusion; for breast PDX models, high copy number of FGFR2 and high expression of FGFR2 and/or the presence of an FGFR fusion. Tumors with activating mutations in other oncogenes (such as KRAS, EGFR, MET) were excluded, as were tumors with high MET expression (> mean of that tumor type). Mice were implanted with tumor fragments and animals selected based on good tumor take and growth. Tumor-bearing mice were orally dosed with vehicle or PRN1371 at a dose of 15 mg/kg b.i.d. Significant tumor growth inhibition was observed in three of the four squamous NSCLC PDX models (Table 3). In two PDX models, BN2289 and LI1055, tumor regression was observed.

The effects of treatment interruption were assessed in LI1055, a mixed liver carcinoma exhibiting an FGFR2:CCDC6 fusion. In this model, PRN1371 oral dosing for 28 days resulted in near complete regression (Fig. 3F). Upon cessation of PRN1371 dosing, the tumor began to regrow, yet upon reinitiation of daily oral dosing with PRN1371, the tumor again responded with the tumor size returning toward baseline. Hence, the tumor remained sensitive to PRN1371 after the initial dosing period. In summary, strong antitumor activity exhibited by PRN1371 across various PDX tumor models strongly suggests that PRN1371 will have a significant impact across diverse tumor types.

Discussion

Genetic alterations of FGFRs, including mutations, fusions, and amplification, can lead to constitutive pathway activation, thus driving cancer growth. Several FGFR inhibitors currently undergoing clinical trials have shown promising responses in FGFR3-mutant urothelial cancer and FGFR1-amplified squamous NSCLC (7, 11). In this work, we describe the covalent FGFR1-4 inhibitor PRN1371. PRN1371 was highly potent toward FGFR1-4 in both biochemical and cellular assays, was strongly selective for FGFR, exhibited potent antiproliferative activity across various cancer cell lines harboring different FGFR alterations, and exhibited antitumor activity in a variety of tumor xenograft and PDX models driven by FGFR alterations in response to both continuous and intermittent dosing paradigms.

This is the first publication describing the preclinical pharmacology of a highly selective covalent FGFR1-4 inhibitor that has progressed to a phase I dose escalation. While in the past a covalent inhibitor approach was considered to be a challenge for achieving an adequate efficacy–tolerability balance in the

clinic, in the last few years several covalent protein kinase inhibitors have demonstrated high clinical efficacy for several cancer types with a manageable side effect profile. For instance, second- and third-generation EGFR/HER-family covalent inhibitors have entered clinical studies, with afatinib and osimertinib now approved for a subset of patients with metastatic NSCLC expressing EGFR mutations (12, 13). Ibrutinib, a covalent inhibitor of Bruton tyrosine kinase (BTK), has been approved for chronic lymphocytic leukemia, mantle cell lymphoma, Waldenstrom's macroglobulinemia, and marginal zone lymphoma with multiple additional covalent BTK inhibitors now undergoing clinical evaluation (14).

In this work, several experiments were performed to establish that PRN1371 forms an irreversible covalent bond with an active-site cysteine of FGFR, leading to sustained pathway inhibition. Inhibition of FGFR1 by PRN1371 was sustained during an extended period of dialysis, during which noncovalent inhibitors dissociated from FGFR1 allowing kinase activity to return. In addition, PRN1371, but not a noncovalent inhibitor, demonstrated sustained inhibition of FGFR2 in SNU16 cells following inhibitor washout as evidenced by sustained block in FGFR2 phosphorylation. This was further confirmed *in vivo* with sustained pathway inhibition achieved in tumors treated with PRN1371 beyond the time PRN1371 was detectable in circulation.

PRN1371 exhibited striking potency against cancer cell lines harboring FGFR alterations, including gastric and bladder cancer cell lines exhibiting either an FGFR3 fusion or FGFR2 amplification, respectively. Furthermore, robust antitumor activity was observed in various tumor xenograft and PDX models. PRN1371 demonstrated robust tumor growth inhibition in SNU16 and RT4 xenograft studies, with regression observed in RT4 at a low dose. In order to explore whether efficacy could be maintained with intermittent dosing, efficacy was assessed in the SNU16 xenograft model with either an intermittent dosing regimen or a high bolus dose for a shorter period of time and both regimens resulted in robust tumor growth inhibition and even tumor regression.

As PDX models are highly predictive of responses observed in the clinic, PRN1371 was assessed in various PDX models of different cancer lineages and harboring different FGFR alterations. A range of antitumor activity was observed, with both modest and robust tumor growth inhibition across various squamous NSCLC PDX models, including regression for PDX models BN2289 and LI1055. Disruption of dosing followed by reinitiation of dosing still resulted in reduced tumor growth in LI1055, suggesting that intermittent dosing could be considered for clinical dosing regiments to enable efficacious and tolerated responses. Additional cancer types exhibiting FGFR alterations beyond those tested in this paper may also show robust responses to PRN1371, including bladder, cholangiocarcinoma, and squamous head and neck cancer. Indeed, striking clinical responses to FGFR inhibitors, such as BGJ398 and JNJ-42756493, have been observed in both cholangiocarcinoma and urothelial cancer, both of which are indications with high unmet medical need (7, 11).

While several selective FGFR inhibitors are making strides in the clinic, no selective FGFR inhibitor has yet to achieve FDA approval. Some of the challenges facing the clinical development of FGFR inhibitors include selecting the right patient that will benefit from an FGFR inhibitor which may vary with different tumor types, managing the toxicity profile of on-target hyperphosphatemia, predicting the mechanisms of acquired resistance that may emerge and designing a rational combination strategy to abrogate this. The first report of a genetic mechanism driving clinical acquired resistance to FGFR inhibition was recently published (15). In a phase II trial of BGJ398 in cholangiocarcinoma patients exhibiting FGFR2 fusions, the initial efficacy was striking but not durable, as driven by the emergence of FGFR2 resistance mutations, including a gatekeeper mutation, V564I. The implication of this clinical observation is that these FGFR2 resistance mutations may also drive intrinsic resistance to FGFR inhibitors and furthermore a similar mechanism of FGFR3 resistance mutations may drive acquired resistance to FGFR3-fusion expressing cancers in response to FGFR inhibition. The emergence of secondary FGFR resistant mutations is comparable to that observed in response to ALK inhibitors in ALK-fusion patients (16), suggesting a strategic approach of developing structurally optimized FGFR inhibitors may be required for durable responses in FGFR-driven cancers. In this strategy, a covalent mechanism may be an advantage based on the assumption that covalent inhibitors exhibit less susceptibility to resistance arising from mutations (17).

Recent clinical data demonstrated a relatively low overall response rate with selective FGFR inhibitors in squamous NSCLC and breast cancer harboring FGFR amplification (7). This raises multiple concerns of whether FGFR amplification is a sole oncogenic driver in different cancer types or whether a certain threshold of FGFR amplification may be necessary to translate into response to FGFR inhibition. In one study involving squamous cancer cell lines, high FGFR1 amplification and high FGFR1 protein expression were found to be more sensitive to FGFR inhibitors compared to those exhibiting low protein expression, suggesting that screening by protein levels may be a better patient selection approach (18). Alternatively, FGFR amplification may be accompanied by additional genetic driver alterations, suggesting that a combination strategy may be critical to improving the incidence of response to FGFR inhibitors in these patients. Certainly, this also points to the challenge of effectively selecting patients; indeed, determining the best screening approach (assessing mRNA vs. protein levels of FGFR) is still being explored in the clinic and it is highly likely that the predictive value of mRNA, DNA, or protein may be dependent on the cancer type or type of FGFR alteration.

In summary, we have developed a potent, selective, covalent FGFR1-4 inhibitor that enables sustained pathway modulation without continuous drug exposure *in vivo* and exhibits strong activity in numerous xenograft and PDX models with both continuous and alternative dosing regimens. PRN1371 is currently under investigation in a phase I clinical study (NCT02608125) in patients with advanced solid tumors.

Disclosure of Potential Conflicts of Interest

K.A. Brameld, T.D. Owens, R.J. Hill, and D.M. Goldstein have ownership interest (including patents) in Principia Biopharma. Y. Xing is a scientist at Principia Biopharma. No potential conflicts of interest were disclosed by the other authors.

Authors' Contributions

Conception and design: K.A. Brameld, E. Verner, R.J. Hill, M.E. Gerritsen, D.M. Goldstein, J.M. Bradshaw

Development of methodology: K.A. Brameld, V.T. Phan, T.D. Owens, Y. Xing, R.J. Hill, M.E. Gerritsen, J.M. Bradshaw
Acquisition of data (provided animals, acquired and managed patients, provided facilities, etc.): E. Venetsanakos, V.T. Phan, T.D. Owens, D. Tam, J. LaStant, K. Leung, D.E. Karr, M.E. Gerritsen, J.M. Bradshaw
Analysis and interpretation of data (e.g., statistical analysis, biostatistics, computational analysis): E. Venetsanakos, K.A. Brameld, V.T. Phan, Y. Xing, J. LaStant, D.E. Karr, M.E. Gerritsen, D.M. Goldstein, J.O. Funk, J.M. Bradshaw
Writing, review, and/or revision of the manuscript: E. Venetsanakos, K.A. Brameld, V.T. Phan, J. LaStant, D.E. Karr, R.J. Hill, M.E. Gerritsen, D.M. Goldstein, J.M. Bradshaw
Administrative, technical, or material support (i.e., reporting or organizing data, constructing databases): J. LaStant, J.M. Bradshaw
Study supervision: E. Venetsanakos, K.A. Brameld, V.T. Phan, J. LaStant, J.O. Funk, J.M. Bradshaw

The costs of publication of this article were defrayed in part by the payment of page charges. This article must therefore be hereby marked *advertisement* in accordance with 18 U.S.C. Section 1734 solely to indicate this fact.

Received April 6, 2017; revised July 11, 2017; accepted September 22, 2017; published OnlineFirst October 4, 2017.

References

1. Lieu C, Heymach J, Overman M, Tran H, Kopetz S. Beyond VEGF: inhibition of the fibroblast growth factor pathway and antiangiogenesis. Clin Cancer Res 2011;17:6130–9.
2. Owen BM, Mangelsdorf DJ, Kliewer SA. Tissue-specific actions of the metabolic hormones FGF15/19 and FGF21. Trends Endocrinol Metab 2015;26:22–9.
3. Turner N, Grose R. Fibroblast growth factor signalling: from development to cancer. Nat Rev Cancer 2010;10:116–29.
4. Gallo LH, Nelson KN, Meyer AN, Donoghue DJ. Functions of fibroblast growth factor receptors in cancer defined by novel translocations and mutations. Cytokine Growth Factor Rev 2015;26:425–49.
5. Touat M, Ileana E, Postel-Vinay S, André F, Soria JC. Targeting FGFR signaling in cancer. Clin Cancer Res 2015;21:2684–94.
6. Hierro C, Rodon J, Tabernero J. Fibroblast growth factor (FGF) receptor/FGF inhibitors: novel targets and strategies for optimization of response of solid tumors. Semin Oncol 2015;42:801–19.
7. Nogova L, Sequist LV, Perez Garcia JM, Andre F, Delord JP, Hidalgo M, et al. Evaluation of BGJ398, a fibroblast growth factor receptor 1-3 kinase inhibitor, in patients with advanced solid tumors harboring genetic alterations in fibroblast growth factor receptors: results of a global phase I, dose-escalation and dose-expansion study. J Clin Oncol 2017;35:157–65.
8. Brameld KA, Owens TD, Verner E, Venetsanakos E, Bradshaw JM, Phan VT, et al. Discovery of the irreversible covalent FGFR1-4 inhibitor 8-(3-(4-acryloylpiperazin-1-yl)propyl)-6-(2,6-dichloro-3,5-dimethoxyphenyl)-2-(methylamino)pyrido[2,3-d]pyrimidin-7(8H)-one (PRN1371) for the treatment of solid tumors. J Med Chem 2017;60:6516–27.
9. Gao H, Korn JM, Ferretti S, Monahan JE, Wang Y, Singh M, et al. High-throughput screening using patient-derived tumor xenografts to predict clinical trial drug response. Nat Med 2015;21:1318–25.
10. Byrne AT, Alférez DG, Amant F, Annibali D, Arribas J, Biankin AV, et al. Interrogating open issues in cancer precision medicine with patient-derived xenografts. Nat Rev Cancer 2017;17:254–68.
11. Tabernero J, Bahleda R, Dienstmann R, Infante JR, Mita A, Italiano A, et al. Phase I dose-escalation study of JNJ-42756493, an oral pan-fibroblast growth factor receptor inhibitor, in patients with advanced solid tumors. J Clin Oncol 2015;33:3401–8.
12. Sullivan I, Planchard D. Next-generation EGFR tyrosine kinase inhibitors for treating EGFR-mutant lung cancer beyond first line. Front Med (Lausanne) 2016;3:76.
13. Mok TS, Wu YL, Ahn MJ, Garassino MC, Kim HR, Ramalingam SS, et al. Osimertinib or platinum-pemetrexed in EGFR T790M-positive lung cancer. N Engl J Med 2017;376:629–40.
14. de Claro RA, McGinn KM, Verdun N, Lee SL, Chiu HJ, Saber H, et al. FDA approval: ibrutinib for patients with previously treated mantle cell lymphoma and previously treated chronic lymphocytic leukemia. Clin Cancer Res 2015;21:3586–90.
15. Goyal L, Saha SK, Liu LY, Siravegna G, Leshchiner I, Ahronian LG, et al. Polyclonal secondary FGFR2 mutations drive acquired resistance to FGFR inhibition in patients with FGFR2 fusion-positive cholangiocarcinoma. Cancer Discov 2017;7:252–63.
16. Lin JJ, Riely GJ, Shaw AT. Targeting ALK: precision medicine takes on drug resistance. Cancer Discov 2017;7:137–55.
17. Barf T, Kaptein A. Irreversible protein kinase inhibitors: balancing the benefits and risks. J Med Chem 2012;55:6243–62.
18. Kotani H, Ebi H, Kitai H, Nanjo S, Kita K, Huynh TG, et al. Co-active receptor tyrosine kinases mitigate the effect of FGFR inhibitors in FGFR1-amplified lung cancers with low FGFR1 protein expression. Oncogene 2016;35:3587–97.